Acta Mech 226, 2089–2101 (2015)
DOI 10.1007/s00707-015-1303-9

Tian-shu Song · Ahmed Hassan

Dynamic anti-plane analysis for symmetrically radial cracks near a non-circular cavity in piezoelectric bi-materials

Received: 9 August 2014 / Revised: 9 December 2014 / Published online: 28 January 2015

Abstract Dynamic incident anti-plane shearing (SH-wave) analysis is considered to calculate the dynamic stress intensity factors (DSIFs) in transversely isotropic piezoelectric bi-materials, which contain symmetrically radial cracks, near the edges of a non-circular cavity. Green's functions are established based on complex variable and conformal mapping methods. Conjunction and crack-deviation techniques are used to evaluate DSIFs at the cracks' tips. Boundary conditions are solved by applying the orthogonal function expansion technique. Models with elliptic cavities are studied numerically based on FORTRAN language program. A comparison is accomplished to adjust program validity. Results clarified the influences on DSIFs under proper conditions.

1 Introduction

In modern science technology, important smart materials as piezoelectric materials are utilized widely. They have very important applications due to their electro-mechanical coupling response. As example, piezoelectric materials have been used to establish many devices in the design and health monitoring of marine structures, such as sensors, actuators and power supplies. But due to materials stiff and brittle nature, the faults and brittleness are occurring during manufacturing, polling process and service procedures. Researchers payed great attention to study the defects behaviors and influences, and how they harm the efficiency and validity of those devices.

In the last few years, the defects existing in piezoelectric materials have been analyzed in various arrangements and loading conditions. For a two-dimensional piezoelectric plate subjected to mechanical and electric load based on conformal mapping technique, Qin [1] developed a Green's function satisfying traction-free and exact electric boundary conditions along a hole. Wu [2] developed an effective method to study a crack in a confocal elliptic piezoelectric in-homogeneity embedded in an infinite piezoelectric medium. Liu and Wang [3] analyzed the electro-elastic interaction of a screw dislocation and a notch in a piezoelectric bi-material. Sasaki et al. [4] performed an analysis on transversely isotropic piezoelectric materials containing an arbitrarily shaped boundary at infinity, using the complex variable function method. Gui et al. [5] studied the problem of collinear periodic cracks in an infinite piezoelectric body by means of the Stroh formalism. Guo et al. [6] investigated the problem of two non-symmetrical collinear cracks emanating from an elliptical hole in a

T. Song
College of Aerospace and Civil Engineering, Harbin Engineering University, Harbin, China
E-mail: songts@126.com
Tel.: +86-13895787972

A. Hassan (✉)
Department of Civil Engineering, MTC, Cairo, Egypt
E-mail: ahmed_hassan_mohamed@hotmail.com
Tel.: +86-18246048752

piezoelectric solid based on the Stroh-type formalism. Also, they considered the fracture behavior of multiple cracks emanating from a circular hole in piezoelectric materials using the complex variable function method [7].

For scattering of SH-waves and dynamic stress concentration under the complex function method, Chen et al. [8] investigated the cases at bi-material structures that possess an interface elliptic cavity, by using Green's function. Liu and Chen [9] investigated cases by radial cracks of any limited length along the radius originating at the boundary of an elliptical hole, using Green's function. Liu and Lin [10] constructed a suitable Green's function for cases of an interacting interface crack and a circular cavity near a bi-material interface.

For anti-plane mechanical and in-plane electric loading based on conformal mapping technique, Wu and Dzenis [11] studied an interfacial edge crack in a piezoelectric bi-material wedge interacting with a screw dislocation. Chen et al. [12] presented a novel efficient procedure to analyze the elliptical in-homogeneity problem in piezoelectric materials, using Green's function.

Recently, based on the complex variable method combined with the method of conformal mapping, Rogowski [13] considered that in the mode III two asymmetrical edge cracks emanate from an elliptical hole problem in a medium possessing coupled electro-magneto-elasticity. Lu et al. [14] studied the fracture problem of two semi-infinite collinear cracks in a piezoelectric strip under the anti-plane shear stress and the in-plane electric load. Also, Guo and Lu [15] investigated the problem of two non-symmetrical collinear cracks emanating from an elliptical hole in a piezoelectric solid based on the Stroh-type formalism and conformal mapping technique. Xiao et al. [16] investigated piezoelectric materials with a doubly periodic array of cracks and rigid-line inclusions by employing the conformal mapping technique and the elliptical function theory.

The dynamic incident anti-plane shearing (SH-wave) analysis is considered in the present paper to calculate theoretically the dynamic stress intensity factors (DSIFs) in transversely isotropic piezoelectric bi-materials, which contain symmetrically radial cracks, near the edges of a non-circular cavity. The objective of the paper is placed on obtaining DSIFs at the cracks' inner and outer tips based on complex variable and conformal mapping methods by conjunction and crack-division techniques. The boundary conditions are solved by applying the orthogonal function expansion technique. By applying FORTRAN language program, numerical models with elliptic cavities are studied for different elliptic axial length ratios, different wave numbers, and different piezoelectric parameters. Also, a comparison is shown to adjust program validity. Results clarified the influences on DSIFs which affect the efficiency of piezoelectric devices and materials under proper conditions.

2 Fundamental equations

Consider two symmetric interfacial cracks near the edges of a non-circular cavity, at transversely isotropic semi-infinite piezoelectric media PM_I and PM_{II} in the XY-plane. The poling direction is the positive Z-axis. As it is clear in Fig. 1, A represents the cracks' lengths, and B represents the distances between the cavity edges and the cracks' inner tips. The positions of the left crack's inner and outer tips are η_1 and η_2, respectively. The model is subjected to a dynamic SH-wave. The time-harmonic and the two-dimensional field can be expressed by the following equation:

$$F^*(X, Y, t) = F(X, Y)\mathrm{e}^{-i\omega t} \tag{1}$$

where F^* is the desired field variable and ω is the incident wave frequency. For the sake of convenience, the time-independent variable $F(X, Y)$ will be accounted in all the following equations neglecting the exponential $\mathrm{e}^{-i\omega t}$ [17].

Fundamental equations of linear piezoelectricity under an SH-wave effect, in the absence of body forces and free charges, can be specified as

$$c_{44}\nabla^2 w + e_{15}\nabla^2\phi + \rho\omega^2 w = 0, \qquad e_{15}\nabla^2 w - \kappa_{11}\nabla^2\phi = 0 \tag{2}$$

where c_{44}, e_{15} and κ_{11} are shear elastic modulus, piezoelectric constant and dielectric constant of the piezoelectric medium, respectively, while w, ϕ and ρ are out-of-plane displacement, electric potential and mass density of the medium, respectively.

Based on the conformal mapping method and by using complex variables $X + iY = \omega(\eta)$, $X - iY = \overline{\omega(\eta)}$, the external field of a non-circular cavity in the XY-plane can be transformed into one outside of a unit circle in the η-plane, if only $\omega'(\eta) \neq 0$ [17]. The mapping domain expressed by the column coordinate system (r, θ)

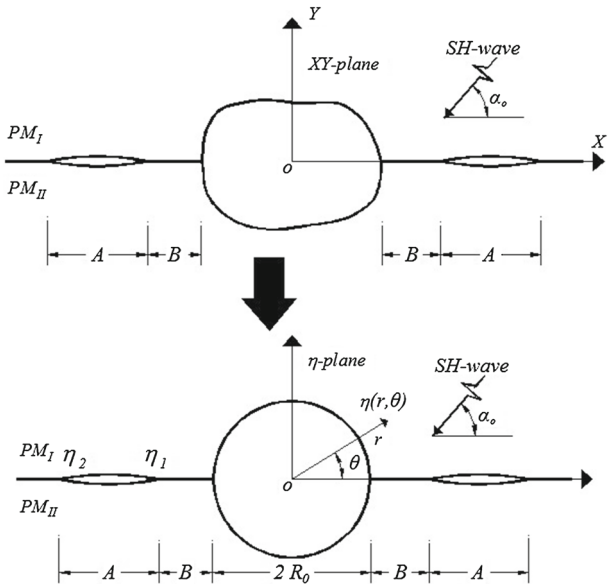

Fig. 1 Piezoelectric bi-materials with symmetrically interfacial cracks near a non-circular cavity and the equivalent mapping plane

is centered at the origin-o, where $\eta = re^{i\theta}$ and $R_0 = 1$ is the circular cavity radius as shown in Fig. 1. In this case, the fundamental equations (2) can be simplified further as:

$$\frac{\partial^2 w}{\partial \eta \partial \overline{\eta}} = \left(\frac{ik}{2}\right)^2 \omega'(\eta)\overline{\omega'(\eta)}\omega(\eta, \overline{\eta}), \qquad \frac{\partial^2 f}{\partial \eta \partial \overline{\eta}} = 0 \tag{3}$$

where $k = \omega\sqrt{\rho/c^*}$ is the wave number, $c^* = c_{44}(1 + \lambda)$ is the effective piezoelectric stiffness, and $\lambda = e_{15}^2/c_{44}\kappa_{11}$ is the dimensionless piezoelectric parameter of the medium.

The electric potential can be defined by

$$\phi = \frac{e_{15}}{\kappa_{11}} w + f. \tag{4}$$

Then, the anti-plane shear stress components (τ_{rz} and $\tau_{\theta z}$) and the in-plane electric displacement components (D_r and D_θ) for a piezoelectric solid can be expressed by:

$$\begin{aligned}
\tau_{rz} &= \frac{c^*}{|\omega'(\eta)|}\left(\frac{\partial w}{\partial \eta}e^{i\theta} + \frac{\partial w}{\partial \overline{\eta}}e^{-i\theta}\right) + \frac{e_{15}}{|\omega'(\eta)|}\left(\frac{\partial f}{\partial \eta}e^{i\theta} + \frac{\partial f}{\partial \overline{\eta}}e^{-i\theta}\right), \\
\tau_{\theta z} &= \frac{ic^*}{|\omega'(\eta)|}\left(\frac{\partial w}{\partial \eta}e^{i\theta} - \frac{\partial w}{\partial \overline{\eta}}e^{-i\theta}\right) + \frac{ie_{15}}{|\omega'(\eta)|}\left(\frac{\partial f}{\partial \eta}e^{i\theta} - \frac{\partial f}{\partial \overline{\eta}}e^{-i\theta}\right),
\end{aligned} \tag{5}$$

$$\begin{aligned}
D_r &= -\frac{\kappa_{11}}{|\omega'(\eta)|}\left(\frac{\partial f}{\partial \eta}e^{i\theta} + \frac{\partial f}{\partial \overline{\eta}}e^{-i\theta}\right), \\
D_\theta &= -\frac{i\kappa_{11}}{|\omega'(\eta)|}\left(\frac{\partial f}{\partial \eta}e^{i\theta} - \frac{\partial f}{\partial \overline{\eta}}e^{-i\theta}\right).
\end{aligned} \tag{6}$$

3 Green's functions and boundary conditions

Green's functions of elastic displacement G_w and electric potential G_ϕ for a semi-infinite piezoelectric medium, under a dynamic incident SH-wave at an arbitrary point η_0 with angle θ_0, can be described, respectively, as [8,9]:

$$G_w = \frac{i}{2c^*} H_0^{(1)}(k|\omega(\eta) - \omega(\eta_0)|) + \sum_{n=0}^{\infty} A_n H_n^{(1)}(k|\omega(\eta)|) \left[\left\{ \frac{\omega(\eta)}{|\omega(\eta)|} \right\}^n + \left\{ \frac{\omega(\eta)}{|\omega(\eta)|} \right\}^{-n} \right], \tag{7}$$

$$G_\phi = \frac{e_{15}}{\kappa_{11}} G_w + \frac{i}{2c^*} \sum_{n=0}^{\infty} \left(B_n \eta^{-n} + C_n \overline{\eta}^{-n} \right) \tag{8}$$

where $H_n^{(1)}$ is the Hankel function of the first kind. In the semicircular cavity, Green's function G_ϕ^c can be described as:

$$G_\phi^c = \frac{i}{2c^*} \left[D_0 + \sum_{n=1}^{\infty} \left(D_n \eta^n + E_n \overline{\eta}^n \right) \right]. \tag{9}$$

Consider that the dynamic incident SH-wave directed with an angle α_0 in medium PM_I and the two interfacial cracks are existing near the edges of a circular cavity in the equivalent mapping plane as shown in Fig. 1. Superscripts I, II and c are used to express variables in PM_I, PM_{II} and the cavity, respectively. Under traction- free and electrically permeable assumptions, the boundary continuity conditions across the medium cavity interface should be as follows [17,18]:

$$\left\{ \begin{array}{l} D_r^{\mathrm{I}} = D_r^c,\ G_\phi^{\mathrm{I}} = G_\phi^c,\ \tau_{rz}^{\mathrm{I}} = 0, \\ D_r^{\mathrm{II}} = D_r^c,\ G_\phi^{\mathrm{II}} = G_\phi^c,\ \tau_{rz}^{\mathrm{II}} = 0 \end{array} \right\}, \quad |\eta| \in 1. \tag{10}$$

Using the orthogonal function expansion technique, unknown coefficients in Green's functions (A_n, B_n, C_n, D_n, E_n and D_0) can be defined by applying the boundary continuity conditions and Hankel function relations [8,17]:

$$\begin{aligned}
\frac{\partial}{\partial \eta} \left[H_n^{(1)}(k|\omega(\eta)|) \left\{ \frac{\omega(\eta)}{|\omega(\eta)|} \right\}^n \right] &= \frac{k}{2} H_{n-1}^{(1)}(k|\omega(\eta)|) \left\{ \frac{\omega(\eta)}{|\omega(\eta)|} \right\}^{n-1} \omega'(\eta), \\
\frac{\partial}{\partial \overline{\eta}} \left[H_n^{(1)}(k|\omega(\eta)|) \left\{ \frac{\omega(\eta)}{|\omega(\eta)|} \right\}^n \right] &= \frac{-k}{2} H_{n+1}^{(1)}(k|\omega(\eta)|) \left\{ \frac{\omega(\eta)}{|\omega(\eta)|} \right\}^{n+1} \overline{\omega'(\eta)}, \\
\frac{\partial}{\partial \eta} \left[H_n^{(1)}(k|\omega(\eta)|) \left\{ \frac{\omega(\eta)}{|\omega(\eta)|} \right\}^{-n} \right] &= \frac{-k}{2} H_{n+1}^{(1)}(k|\omega(\eta)|) \left\{ \frac{\omega(\eta)}{|\omega(\eta)|} \right\}^{-n-1} \omega'(\eta), \\
\frac{\partial}{\partial \overline{\eta}} \left[H_n^{(1)}(k|\omega(\eta)|) \left\{ \frac{\omega(\eta)}{|\omega(\eta)|} \right\}^{-n} \right] &= \frac{k}{2} H_{n-1}^{(1)}(k|\omega(\eta)|) \left\{ \frac{\omega(\eta)}{|\omega(\eta)|} \right\}^{-n+1} \overline{\omega'(\eta)}.
\end{aligned} \tag{11}$$

Then, the following relations can be determined:

$$D_n = -\frac{\kappa_{11}}{\kappa_0} C_n, \qquad E_n = -\frac{\kappa_{11}}{\kappa_0} B_n, \tag{12}$$

$$\begin{aligned}
&\frac{e_{15}}{\kappa_{11}} \sum_{n=0}^{\infty} A_n H_n^{(1)}(k|\omega(\eta)|) \left[\left\{ \frac{\omega(\eta)}{|\omega(\eta)|} \right\}^n + \left\{ \frac{\omega(\eta)}{|\omega(\eta)|} \right\}^{-n} \right] + \frac{i}{2c^*} (1 + \frac{\kappa_{11}}{\kappa_0}) \sum_{n=1}^{\infty} \left(B_n \mathrm{e}^{-in\theta} + C_n \mathrm{e}^{in\theta} \right) \\
&- D_0 = \frac{-e_{15} i}{2\kappa_{11} c^*} H_0^{(1)}(k|\omega(\eta) - \omega(\eta_0)|),
\end{aligned} \tag{13}$$

$$\begin{aligned}
&k \sum_{n=0}^{\infty} A_n \left[H_{n-1}^{(1)}(k|\omega(\eta)|) \left\{ \frac{\omega(\eta)}{|\omega(\eta)|} \right\}^{n-1} - H_{n+1}^{(1)}(k|\omega(\eta)|) \left\{ \frac{\omega(\eta)}{|\omega(\eta)|} \right\}^{-n-1} \right] \omega'(\eta) \mathrm{e}^{i\theta} \\
&- k \sum_{n=0}^{\infty} A_n \left[H_{n+1}^{(1)}(k|\omega(\eta)|) \left\{ \frac{\omega(\eta)}{|\omega(\eta)|} \right\}^{n+1} - H_{n-1}^{(1)}(k|\omega(\eta)|) \left\{ \frac{\omega(\eta)}{|\omega(\eta)|} \right\}^{-n+1} \right] \overline{\omega'(\eta)} \mathrm{e}^{-i\theta} \\
&- \frac{e_{15} n i}{c^{*2}} \sum_{n=1}^{\infty} (B_n \mathrm{e}^{-in\theta} + C_n \mathrm{e}^{in\theta}) = -\frac{ki}{2c^*} H_{-1}^{(1)}(k|\omega(\eta) - \omega(\eta_0)|) \left\{ \frac{\overline{\omega(\eta)} - \overline{\omega(\eta_0)}}{|\omega(\eta) - \omega(\eta_0)|} \right\} \omega'(\eta) \mathrm{e}^{i\theta} \\
&- \frac{ki}{2c^*} H_{-1}^{(1)}(k|\omega(\eta) - \omega(\eta_0)|) \left\{ \frac{\omega(\eta) - \omega(\eta_0)}{|\omega(\eta) - \omega(\eta_0)|} \right\} \overline{\omega'(\eta)} \mathrm{e}^{-i\theta}
\end{aligned} \tag{14}$$

where κ_0 is the permittivity dielectric constant of the vacuum inside the cavity. Multiplying both sides of Eqs. (13) and (14) by the factor $e^{-im\theta}$ where $m = 0, \pm1, \pm2, \ldots$ and integrating them from 0 to 2π about θ, the final relations have the form of an infinite linear algebraic system of equations about the unknown coefficients [17]:

$$\sum_{n=0}^{\infty} A_n P_{ln} + \sum_{n=1}^{\infty} B_n q_{ln} + \sum_{n=1}^{\infty} C_n s_{ln} + D_0 \beta_l = \epsilon_l, \qquad l = 1, 2 \tag{15}$$

in which

$$P_{1n} = \frac{e_{15}}{2\pi\kappa_{11}} \int_0^{2\pi} H_n^{(1)}(k|\omega(\eta)|) \left[\left\{ \frac{\omega(\eta)}{|\omega(\eta)|} \right\}^n + \left\{ \frac{\omega(\eta)}{|\omega(\eta)|} \right\}^{-n} \right] e^{-im\theta} d\theta,$$

$$P_{2n} = \frac{k}{2\pi} \int_0^{2\pi} \left[H_{n-1}^{(1)}(k|\omega(\eta)|) \left\{ \frac{\omega(\eta)}{|\omega(\eta)|} \right\}^{n-1} - H_{n+1}^{(1)}(k|\omega(\eta)|) \left\{ \frac{\omega(\eta)}{|\omega(\eta)|} \right\}^{-n-1} \right] \omega'(\eta) e^{i\theta} e^{-im\theta} d\theta$$
$$- \frac{k}{2\pi} \int_0^{2\pi} \left[H_{n+1}^{(1)}(k|\omega(\eta)|) \left\{ \frac{\omega(\eta)}{|\omega(\eta)|} \right\}^{n+1} - H_{n-1}^{(1)}(k|\omega(\eta)|) \left\{ \frac{\omega(\eta)}{|\omega(\eta)|} \right\}^{-n+1} \right] \overline{\omega'(\eta)} e^{-i\theta} e^{-im\theta} d\theta,$$

$$q_{1n} = \frac{i}{4\pi c^*} \left(1 + \frac{\kappa_{11}}{\kappa_0}\right) \int_0^{2\pi} e^{-in\theta} e^{-im\theta} d\theta,$$

$$q_{2n} = -\frac{e_{15} n i}{2\pi c^{*2}} \int_0^{2\pi} e^{-in\theta} e^{-im\theta} d\theta,$$

$$s_{1n} = \frac{i}{4\pi c^*} \left(1 + \frac{\kappa_{11}}{\kappa_0}\right) \int_0^{2\pi} e^{in\theta} e^{-im\theta} d\theta,$$

$$s_{2n} = -\frac{e_{15} n i}{2\pi c^{*2}} \int_0^{2\pi} e^{in\theta} e^{-im\theta} d\theta,$$

$$\beta_1 = -\frac{1}{2\pi} \int_0^{2\pi} e^{-im\theta} d\theta, \qquad \beta_2 = 0,$$

$$\epsilon_1 = -\frac{e_{15} i}{4\pi c^* \kappa_{11}} \int_0^{2\pi} H_0^{(1)}(k|\omega(\eta) - \omega(\eta_0)|)\, e^{-im\theta} d\theta,$$

$$\epsilon_2 = -\frac{ki}{4\pi c^*} \int_0^{2\pi} H_{-1}^{(1)}(k|\omega(\eta) - \omega(\eta_0)|) \left\{ \frac{\overline{\omega(\eta)} - \overline{\omega(\eta_0)}}{|\omega(\eta) - \omega(\eta_0)|} \right\} \omega'(\eta) e^{i\theta} e^{-im\theta} d\theta,$$
$$- \frac{ki}{4\pi c^*} \int_0^{2\pi} H_{-1}^{(1)}(k|\omega(\eta) - \omega(\eta_0)|) \left\{ \frac{\omega(\eta) - \omega(\eta_0)}{|\omega(\eta) - \omega(\eta_0)|} \right\} \overline{\omega'(\eta)} e^{-i\theta} e^{-im\theta} d\theta.$$

Using the polynomials truncation in Eq. (15) to the Nth term and $m = 0, \pm1, \pm2, \ldots, \pm N$, the relations can be reduced to a finite $4N + 2$ linear algebraic system of equations and $4N + 2$ unknown coefficients. Calculating the reduced relations leads to determine the unknown coefficients. The satisfied calculations can be obtained only by taking $N = 8$.

4 Dynamic electro-elastic fields

At the interface of the piezoelectric bi-materials, different impedances caused scattering phenomena. The dynamic electro-elastic fields and the corresponding scattering fields can be given as follows [8,9]:

1. Incident elastic displacement and electric potential fields in PM_I:

$$w^{(i)} = w_0\, exp\left\{ \frac{-ik_I}{2} \left(\omega(\eta) e^{i\alpha_0} + \overline{\omega(\eta)} e^{-i\alpha_0} \right) \right\}, \qquad \phi^{(i)} = \frac{e_{15}^I}{\kappa_{11}^I} w^{(i)} \tag{16}$$

where w_0 is the magnitude of the incident displacement wave.

2. Reflecting and scattering electro-elastic fields in PM_I:

$$w^{(r)} = w_1 \exp\left\{\frac{-ik_{\rm I}}{2}\left(\omega(\eta)e^{i\alpha_1} + \overline{\omega(\eta)}e^{-i\alpha_1}\right)\right\}, \qquad \phi^{(r)} = \frac{e_{15}^{\rm I}}{\kappa_{11}^{\rm I}} w^{(r)}, \tag{17}$$

$$w^{(s)} = \sum_{n=-\infty}^{\infty}\left(A_n^{(is)} + A_n^{(rs)}\right) H_n^{(1)}(k_{\rm I}|\omega(\eta)|)\left\{\frac{\omega(\eta)}{|\omega(\eta)|}\right\}^n,$$

$$\phi^{(s)} = \frac{e_{15}^{\rm I}}{\kappa_{11}^{\rm I}} w^{(s)} + \frac{i}{2c_{\rm I}^*}\left[\sum_{n=1}^{\infty}\left(B_n^{(is)}\eta^{-n} + C_n^{(is)}\overline{\eta}^{-n} + B_n^{(rs)}\eta^{-n} + C_n^{(rs)}\overline{\eta}^{-n}\right)\right] \tag{18}$$

where $w_1$and α_1 are the magnitude and angle of the reflecting displacement wave, respectively.

3. Refracting and scattering electro-elastic fields in PM_{II}:

$$w^{(f)} = w_2 \exp\left\{\frac{-ik_{\rm II}}{2}\left(\omega(\eta)e^{i\alpha_2} + \overline{\omega(\eta)}e^{-i\alpha_2}\right)\right\}, \qquad \phi^{(f)} = \frac{e_{15}^{\rm II}}{\kappa_{11}^{\rm II}} w^{(f)}, \tag{19}$$

$$w^{(fs)} = \sum_{n=-\infty}^{\infty} A_n^{(fs)} H_n^{(1)}(k_{\rm II}|\omega(\eta)|)\left\{\frac{\omega(\eta)}{|\omega(\eta)|}\right\}^n,$$

$$\phi^{(fs)} = \frac{e_{15}^{\rm II}}{\kappa_{11}^{\rm II}} w^{(fs)} + \frac{i}{2c_{\rm II}^*}\left[\sum_{n=1}^{\infty}\left(B_n^{(fs)}\eta^{-n} + C_n^{(fs)}\overline{\eta}^{-n}\right)\right] \tag{20}$$

where $w_2$and α_2 are the magnitude and angle of the refracting displacement wave, respectively.

4. The cavity is assumed to be filled with homogeneous gas or vacuum, and free of forces and surface charges. So, the electric potential inside the cavity can be given as:

$$\phi^{c(is)} = \frac{i}{2c_{\rm I}^*}\left[D_0^{(is)} + \sum_{n=1}^{\infty}\left(D_n^{(is)}\eta^n + E_n^{(is)}\overline{\eta}^n\right)\right],$$

$$\phi^{c(rs)} = \frac{i}{2c_{\rm I}^*}\left[D_0^{(rs)} + \sum_{n=1}^{\infty}\left(D_n^{(rs)}\eta^n + E_n^{(rs)}\overline{\eta}^n\right)\right],$$

$$\phi^{c(fs)} = \frac{i}{2c_{\rm II}^*}\left[D_0^{(fs)} + \sum_{n=1}^{\infty}\left(D_n^{(fs)}\eta^n + E_n^{(fs)}\overline{\eta}^n\right)\right]. \tag{21}$$

The total electro-elastic fields for the two media PM_I andPM_{II} are, respectively:

$$w^{\rm I} = w^{(i)} + w^{(r)} + w^{(s)}, \quad \phi^{\rm I} = \phi^{(i)} + \phi^{(r)} + \phi^{(s)}, \tag{22}$$

$$w^{\rm II} = w^{(f)} + w^{(fs)}, \qquad \phi^{\rm II} = \phi^{(f)} + \phi^{(fs)}. \tag{23}$$

All unknown coefficients for incident, reflecting and refracting fields can also be calculated by using the orthogonal function expansion technique. The boundary continuity conditions across the medium cavity interface should be in the following forms:

$$\left\{\begin{array}{l} D_r^{\rm I} = D_r^c,\ \phi^{\rm I} = \phi^c,\ \tau_{rz}^{\rm I} = 0 \\ D_r^{\rm II} = D_r^c,\ \phi^{\rm II} = \phi^c,\ \tau_{rz}^{\rm II} = 0 \end{array}\right\}, \quad |\eta| \in 1. \tag{24}$$

In case of incident unknown coefficients ($A_n^{(is)}$, $B_n^{(is)}$, $C_n^{(is)}$, $D_n^{(is)}$, $E_n^{(is)}$ and $D_0^{(is)}$), the next relations can be determined:

$$D_n^{(is)} = -\frac{\kappa_{11}^{\rm I}}{\kappa_0} C_n^{(is)}, \qquad E_n^{(is)} = -\frac{\kappa_{11}^{\rm I}}{\kappa_0} B_n^{(is)}, \tag{25}$$

$$\frac{e_{15}^{\mathrm{I}}}{\kappa_{11}^{\mathrm{I}}}\sum_{n=-\infty}^{\infty}A_n^{(is)}H_n^{(1)}(k_{\mathrm{I}}|\omega(\eta)|)\left\{\frac{\omega(\eta)}{|\omega(\eta)|}\right\}^n+\frac{i}{2c_{\mathrm{I}}^*}\left(1+\frac{\kappa_{11}^{\mathrm{I}}}{\kappa_0}\right)\sum_{n=1}^{\infty}\left(B_n^{(is)}\mathrm{e}^{-in\theta}+C_n^{(is)}\mathrm{e}^{in\theta}\right)$$
$$-D_0^{(is)}=\frac{-e_{15}^{\mathrm{I}}}{\kappa_{11}^{\mathrm{I}}}w_0\exp\left\{\frac{-ik_{\mathrm{I}}}{2}\left(\omega(\eta)\mathrm{e}^{i\alpha_0}+\overline{\omega(\eta)}\mathrm{e}^{-i\alpha_0}\right)\right\}, \tag{26}$$

$$k_{\mathrm{I}}\sum_{n=-\infty}^{\infty}A_n^{(is)}\left[H_{n-1}^{(1)}(k_{\mathrm{I}}|\omega(\eta)|)\left\{\frac{\omega(\eta)}{|\omega(\eta)|}\right\}^{n-1}\omega'(\eta)\mathrm{e}^{i\theta}-H_{n+1}^{(1)}(k_{\mathrm{I}}|\omega(\eta)|)\left\{\frac{\omega(\eta)}{|\omega(\eta)|}\right\}^{n+1}\overline{\omega'(\eta)}\mathrm{e}^{-i\theta}\right]$$
$$-\frac{e_{15}^{\mathrm{I}}\,ni}{c_{\mathrm{I}}^{*2}}\sum_{n=1}^{\infty}\left(B_n^{(is)}\mathrm{e}^{-in\theta}+C_n^{(is)}\mathrm{e}^{in\theta}\right)=ik_{\mathrm{I}}w_0\exp\left\{\frac{-ik_{\mathrm{I}}}{2}\left(\omega(\eta)\mathrm{e}^{i\alpha_0}+\overline{\omega(\eta)}\mathrm{e}^{-i\alpha_0}\right)\right\}$$
$$\times\left\{\mathrm{e}^{i\alpha_0}\omega'(\eta)\mathrm{e}^{i\theta}+\mathrm{e}^{-i\alpha_0}\overline{\omega'(\eta)}\mathrm{e}^{-i\theta}\right\}. \tag{27}$$

The infinite linear algebraic system of equations about the incident unknown coefficients is as follows:

$$\sum_{n=-\infty}^{\infty}A_n^{(is)}P_{ln}+\sum_{n=1}^{\infty}B_n^{(is)}q_{ln}+\sum_{n=1}^{\infty}C_n^{(is)}s_{ln}+D_0^{(is)}\beta_l=\epsilon_l,\qquad l=1,2 \tag{28}$$

in which

$$P_{1n}=\frac{e_{15}^{\mathrm{I}}}{2\pi\kappa_{11}^{\mathrm{I}}}\int_0^{2\pi}H_n^{(1)}(k_{\mathrm{I}}|\omega(\eta)|)\left\{\frac{\omega(\eta)}{|\omega(\eta)|}\right\}^n\mathrm{e}^{-im\theta}\mathrm{d}\theta,$$
$$P_{2n}=\frac{k_{\mathrm{I}}}{2\pi}\int_0^{2\pi}H_{n-1}^{(1)}(k_{\mathrm{I}}|\omega(\eta)|)\left\{\frac{\omega(\eta)}{|\omega(\eta)|}\right\}^{n-1}\omega'(\eta)\mathrm{e}^{i\theta}\mathrm{e}^{-im\theta}\mathrm{d}\theta$$
$$-\frac{k_{\mathrm{I}}}{2\pi}\int_0^{2\pi}H_{n+1}^{(1)}(k_{\mathrm{I}}|\omega(\eta)|)\left\{\frac{\omega(\eta)}{|\omega(\eta)|}\right\}^{n+1}\overline{\omega'(\eta)}\mathrm{e}^{-i\theta}\mathrm{e}^{-im\theta}\mathrm{d}\theta,$$
$$q_{1n}=\frac{i}{4\pi c_{\mathrm{I}}^*}(1+\frac{\kappa_{11}^{\mathrm{I}}}{\kappa_0})\int_0^{2\pi}\mathrm{e}^{-in\theta}\mathrm{e}^{-im\theta}\mathrm{d}\theta,$$
$$q_{2n}=-\frac{e_{15}^{\mathrm{I}}ni}{2\pi c_{\mathrm{I}}^{*2}}\int_0^{2\pi}\mathrm{e}^{-in\theta}\mathrm{e}^{-im\theta}\mathrm{d}\theta,$$
$$s_{1n}=\frac{i}{4\pi c_{\mathrm{I}}^*}(1+\frac{\kappa_{11}^{\mathrm{I}}}{\kappa_0})\int_0^{2\pi}\mathrm{e}^{in\theta}\mathrm{e}^{-im\theta}\mathrm{d}\theta,$$
$$s_{2n}=-\frac{e_{15}^{\mathrm{I}}ni}{2\pi c_{\mathrm{I}}^{*2}}\int_0^{2\pi}\mathrm{e}^{in\theta}\mathrm{e}^{-im\theta}\mathrm{d}\theta,$$
$$\beta_1=-\frac{1}{2\pi}\int_0^{2\pi}\mathrm{e}^{-im\theta}\mathrm{d}\theta,\qquad\beta_2=0,$$
$$\epsilon_1=-\frac{e_{15}^{\mathrm{I}}w_0}{2\pi\kappa_{11}^{\mathrm{I}}}\int_0^{2\pi}\exp\left\{\frac{-ik_{\mathrm{I}}}{2}\left(\omega(\eta)\mathrm{e}^{i\alpha_0}+\overline{\omega(\eta)}\mathrm{e}^{-i\alpha_0}\right)\right\}\mathrm{e}^{-im\theta}\mathrm{d}\theta,$$
$$\epsilon_2=-\frac{k_{\mathrm{I}}w_0i}{2\pi}\int_0^{2\pi}\exp\left\{\frac{-ik_{\mathrm{I}}}{2}\left(\omega(\eta)\mathrm{e}^{i\alpha_0}+\overline{\omega(\eta)}\mathrm{e}^{-i\alpha_0}\right)\right\}.\left\{\mathrm{e}^{i\alpha_0}\omega'(\eta)\mathrm{e}^{i\theta}+\mathrm{e}^{-i\alpha_0}\overline{\omega'(\eta)}\mathrm{e}^{-i\theta}\right\}\mathrm{e}^{-im\theta}\mathrm{d}\theta.$$

The incident unknown coefficients can be calculated by using the polynomials truncation in Eq. (28) by the same procedure as Eq. (15). Also, the same procedures can be followed to calculate the unknown coefficients for the reflecting field ($A_n^{(rs)}$, $B_n^{(rs)}$, $C_n^{(rs)}$, $D_n^{(rs)}$, $E_n^{(rs)}$ and $D_0^{(rs)}$) and the unknown coefficients for the refracting field ($A_n^{(fs)}$, $B_n^{(fs)}$, $C_n^{(fs)}$, $D_n^{(fs)}$, $E_n^{(fs)}$ and $D_0^{(fs)}$).

5 Integral equation and DSIFs

The conjunction and crack-deviation techniques are used to determine the integral equation and DSIFs at the cracks' inner and outer tips. The piezoelectric bi-materials' conjunction is shown in Fig. 2.

The interface intervals in the mapping plane can be defined as:

$$\left\{\begin{array}{ll} \Gamma_1 \in [R_0,\, R_0+B],\theta=\pi, & \Gamma_2 > R_0+B+A,\theta=\pi, \\ \Gamma_3 \in [R_0,\, R_0+B],\theta=0, & \Gamma_4 > R_0+B+A,\theta=0, \\ C_1 \in [R_0+B,\, R_0+B+A],\theta=\pi, & \\ C_2 \in [R_0+B,\, R_0+B+A],\theta=0 & \end{array}\right\}. \tag{29}$$

To apply the crack-deviation technique, two negative shear stresses $-\tau^{\mathrm{I}}_{\theta z}$ and $-\tau^{\mathrm{II}}_{\theta z}$ are estimated at the cracks locations. The continuity conditions of shear stresses excluding the areas of the cracks and the cavity can be expressed by [9,18]:

$$\tau^{\mathrm{I}}_{\theta z}\cos\theta_0 + f_1(r_0,\theta_0) = \tau^{\mathrm{II}}_{\theta z}\cos\theta_0 + f_2(r_0,\theta_0), \qquad \text{at } \Gamma_1,\Gamma_2,\Gamma_3 \text{ and } \Gamma_4 \tag{30}$$

where $f_1(r_0,\theta_0)$ and $f_2(r_0,\theta_0)$ are two additional stresses applied at the well-bounded interfaces. Returning to Eq. (3), it can be concluded that:

$$\tau^{\mathrm{I}}_{\theta z} = \tau^{(i)}_{\theta z} + \tau^{(r)}_{\theta z} + \tau^{(s)}_{\theta z}, \qquad \tau^{\mathrm{II}}_{\theta z} = \tau^{(f)}_{\theta z} + \tau^{(fs)}_{\theta z} \tag{31}$$

in which

$$\tau^{(i)}_{\theta z} = \frac{k_{\mathrm{I}} c^*_{\mathrm{I}} w_0}{2|\omega'(\eta)|}\left[\exp\left\{\frac{-ik_{\mathrm{I}}}{2}\left(\omega(\eta)\mathrm{e}^{i\alpha_0} + \overline{\omega(\eta)}\mathrm{e}^{-i\alpha_0}\right)\right\}.\left\{\mathrm{e}^{i\alpha_0}\omega'(\eta)\mathrm{e}^{i\theta} - \mathrm{e}^{-i\alpha_0}\overline{\omega'(\eta)}\mathrm{e}^{-i\theta}\right\}\right],$$

$$\tau^{(r)}_{\theta z} = \frac{k_{\mathrm{I}} c^*_{\mathrm{I}} w_1}{2|\omega'(\eta)|}\left[\exp\left\{\frac{-ik_{\mathrm{I}}}{2}\left(\omega(\eta)\mathrm{e}^{i\alpha_1} + \overline{\omega(\eta)}\mathrm{e}^{-i\alpha_1}\right)\right\}.\left\{\mathrm{e}^{i\alpha_1}\omega'(\eta)\mathrm{e}^{i\theta} - \mathrm{e}^{-i\alpha_1}\overline{\omega'(\eta)}\mathrm{e}^{-i\theta}\right\}\right],$$

$$\tau^{(s)}_{\theta z} = \frac{ik_{\mathrm{I}} c^*_{\mathrm{I}}}{2|\omega'(\eta)|}\sum_{n=-\infty}^{\infty}(A^{(is)}_n + A^{(rs)}_n)\left[H^{(1)}_{n-1}(k_{\mathrm{I}}|\omega(\eta)|)\left\{\frac{\omega(\eta)}{|\omega(\eta)|}\right\}^{n-1}\omega'(\eta)\mathrm{e}^{i\theta}\right.$$
$$\left. + H^{(1)}_{n+1}(k_{\mathrm{I}}|\omega(\eta)|)\left\{\frac{\omega(\eta)}{|\omega(\eta)|}\right\}^{n+1}\overline{\omega'(\eta)}\mathrm{e}^{-i\theta}\right]$$

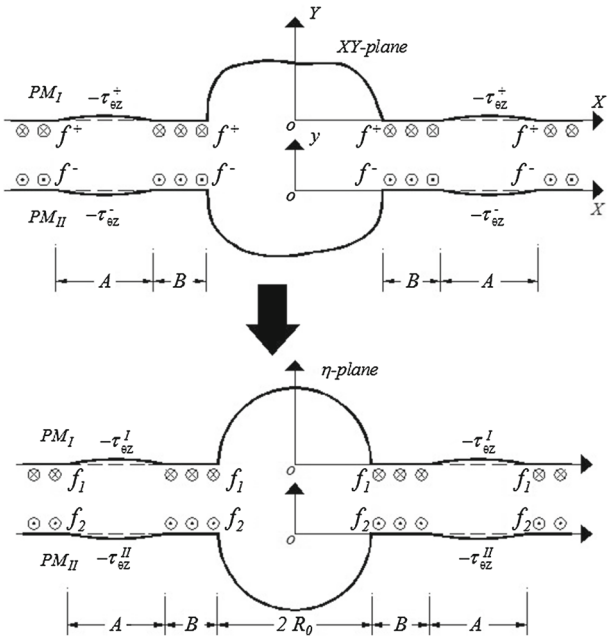

Fig. 2 Piezoelectric bi-materials' conjunction with two semi-non-circular cavities and the equivalent mapping plane

$$+\frac{e_{15}^{\mathrm{I}} n}{2c_{\mathrm{I}}^{*}|\omega'(\eta)|}\sum_{n=1}^{\infty}\left(B_n^{(is)}\mathrm{e}^{-in\theta}-C_n^{(is)}\mathrm{e}^{in\theta}+B_n^{(rs)}\mathrm{e}^{-in\theta}-C_n^{(rs)}\mathrm{e}^{in\theta}\right)$$

$$\tau_{\theta z}^{(f)}=\frac{k_{\mathrm{II}}c_{\mathrm{II}}^{*}w_2}{2|\omega'(\eta)|}\left[\exp\left\{\frac{-ik_{\mathrm{II}}}{2}\left(\omega(\eta)\mathrm{e}^{i\alpha_2}+\overline{\omega(\eta)}\mathrm{e}^{-i\alpha_2}\right)\right\}\cdot\left\{\mathrm{e}^{i\alpha_2}\omega'(\eta)\mathrm{e}^{i\theta}-\mathrm{e}^{-i\alpha_2}\overline{\omega'(\eta)}\mathrm{e}^{-i\theta}\right\}\right]$$

$$\tau_{\theta z}^{(fs)}=\frac{ik_{\mathrm{II}}c_{\mathrm{II}}^{*}}{2|\omega'(\eta)|}\sum_{n=-\infty}^{\infty}A_n^{(fs)}\left[H_{n-1}^{(1)}(k_{\mathrm{II}}|\omega(\eta)|)\left\{\frac{\omega(\eta)}{|\omega(\eta)|}\right\}^{n-1}\omega'(\eta)\mathrm{e}^{i\theta}\right.$$

$$\left.+H_{n+1}^{(1)}(k_{\mathrm{II}}|\omega(\eta)|)\left\{\frac{\omega(\eta)}{|\omega(\eta)|}\right\}^{n+1}\overline{\omega'(\eta)}\mathrm{e}^{-i\theta}\right]+\frac{e_{15}^{\mathrm{II}} n}{2c_{\mathrm{II}}^{*}|\omega'(\eta)|}\sum_{n=1}^{\infty}\left(B_n^{(fs)}\mathrm{e}^{-in\theta}-C_n^{(fs)}\mathrm{e}^{in\theta}\right).$$

The continuity conditions of elastic displacements can be expressed by [18]:

$$w^{\mathrm{I}}(r,\theta)+w^{(f_1)}(r,\theta)+w^{(c_r\mathrm{I})}(r,\theta)=w^{\mathrm{II}}(r,\theta)+w^{(f_2)}(r,\theta)+w^{(c_r\mathrm{II})}(r,\theta) \tag{32}$$

in which

$$w^{(f_1)}=\int_{\Gamma_1\&\Gamma_2}f_1(r_0,\pi)G_w^{\mathrm{I}}(r,\theta;r_0,\pi)\mathrm{d}r_0+\int_{\Gamma_3\&\Gamma_4}f_1(r_0,0)G_w^{\mathrm{I}}(r,\theta;r_0,0)\mathrm{d}r_0,$$

$$w^{(f_2)}=-\int_{\Gamma_1\&\Gamma_2}f_2(r_0,\pi)G_w^{\mathrm{II}}(r,\theta;r_0,\pi)\mathrm{d}r_0-\int_{\Gamma_3\&\Gamma_4}f_2(r_0,0)G_w^{\mathrm{II}}(r,\theta;r_0,0)\mathrm{d}r_0,$$

$$w^{(c_rI)}=\int_{C_1}\tau_{\theta z}^{\mathrm{I}}(r_0,\pi)G_w^{\mathrm{I}}(r,\theta;r_0,\pi)\mathrm{d}r_0-\int_{C_2}\tau_{\theta z}^{\mathrm{I}}(r_0,0)G_w^{\mathrm{I}}(r,\theta;r_0,0)\mathrm{d}r_0,$$

$$w^{(c_rII)}=-\int_{C_1}\tau_{\theta z}^{\mathrm{II}}(r_0,\pi)G_w^{\mathrm{II}}(r,\theta;r_0,\pi)\mathrm{d}r_0+\int_{C_2}\tau_{\theta z}^{\mathrm{II}}(r_0,0)G_w^{\mathrm{II}}(r,\theta;r_0,0)\mathrm{d}r_0.$$

Gathering all the equations above, the final integral equation can be expressed as follows [18]:

$$\begin{aligned}
&\int_{\Gamma_1\&\Gamma_2}f_1(r_0,\pi)\left[G_w^{\mathrm{I}}(r,\theta;r_0,\pi)+G_w^{\mathrm{II}}(r,\theta;r_0,\pi)\right]\mathrm{d}r_0\\
&\quad+\int_{\Gamma_3\&\Gamma_4}f_1(r_0,0)\left[G_w^{\mathrm{I}}(r,\theta;r_0,0)+G_w^{\mathrm{II}}(r,\theta;r_0,0)\right]\mathrm{d}r_0\\
&=\int_{\Gamma_1\&\Gamma_2}\left[\tau_{\theta z}^{\mathrm{I}}(r_0,\pi)-\tau_{\theta z}^{\mathrm{II}}(r_0,\pi)\right]G_w^{\mathrm{II}}(r,\theta;r_0,\pi)\mathrm{d}r_0\\
&\quad-\int_{\Gamma_3\&\Gamma_4}\left[\tau_{\theta z}^{\mathrm{I}}(r_0,0)-\tau_{\theta z}^{\mathrm{II}}(r_0,0)\right]G_w^{\mathrm{II}}(r,\theta;r_0,0)\mathrm{d}r_0\\
&\quad-\int_{C_1}\tau_{\theta z}^{\mathrm{I}}(r_0,\pi)G_w^{\mathrm{I}}(r,\theta;r_0,\pi)\mathrm{d}r_0-\int_{C_1}\tau_{\theta z}^{\mathrm{II}}(r_0,\pi)G_w^{\mathrm{II}}(r,\theta;r_0,\pi)\mathrm{d}r_0\\
&\quad+\int_{C_2}\tau_{\theta z}^{\mathrm{I}}(r_0,0)G_w^{\mathrm{I}}(r,\theta;r_0,0)\mathrm{d}r_0+\int_{C_2}\tau_{\theta z}^{\mathrm{II}}(r_0,0)G_w^{\mathrm{II}}(r,\theta;r_0,0)\mathrm{d}r_0\\
&\quad-w^{(s)}(r,\theta)+w^{(fs)}(r,\theta),\qquad\theta=0,\pi.
\end{aligned} \tag{33}$$

Finally, the dimensionless DSIFs (k_3^{σ}) at η_1 and η_2 can be defined by:

$$k_{3\,\eta_1}^{\sigma}=\frac{1}{\tau_0 Q}\left|\lim_{r_0\to R_0+B}f_1(r_0,\pi)\sqrt{2(r_0-R_0-B)}\right|, \tag{34}$$

$$k_{3\,\eta_2}^{\sigma}=\frac{1}{\tau_0 Q}\left|\lim_{r_0\to R_0+B+A}f_1(r_0,\pi)\sqrt{2(r_0-R_0-B-A)}\right| \tag{35}$$

where the characteristic length $Q=\sqrt{A/2}$, and $\tau_0=k_I w_0 c_{\mathrm{I}}^{*}$ refers to the shear stress magnitude of the incident wave [9,18].

6 Numerical examples and discussions

To examine the influences of different parameters on the DSIFs, some calculations are provided based on FORTRAN language program for Eqs. (34) and (35), for piezoelectric bi-materials media with an elliptic cavity. The conformal mapping function, which transforms the domain outside an ellipse in the XY-plane into one outside a unit circle in η-plane is given by [8,9]:

$$X + iY = \omega(\eta) = \frac{a+b}{2}\left(\eta + \frac{a-b}{a+b}\eta^{-1}\right) \tag{36}$$

in which a and b represent the semi-axes' lengths of the ellipse along the X-axis and Y-axis, respectively.

To adjust the FORTRAN program validity, a comparison of DSIFs at η_2 is accomplished between the paper model and the document [18] model with cracks emerging from circular cavity edges as shown in Fig. 3.

The document model is solved without using complex variable and conformal mapping methods. It can be noticed that the two curves are almost swaying in the same manner with the wave number increment, but they did not coincide well. The DSIFs at $k_I a = 1.0$ are quite different. Also, the peak for the current model's curve occurred at about $k_I a = 1.9$ later than the peak for the document model's curve which occurred at $k_I a = 1.6$.

So, using complex variable and conformal mapping methods in the present paper solution causes the wide change in DSIFs. On the other hand, the distance B is very small ($B/a = 0.001$) but still exists as a separation between the cracks and the cavity. It can be concluded that, depending on the medium's geometry and the sequence of calculations, the relation between the cracks and the cavity is altered causing the changes occurring in the values of the DSIFs.

Divergences of DSIFs at η_1 and η_2 for different semi-axes' percentages of the ellipse are shown in Fig. 4. The outer tip gave the larger values of DSIFs than the inner tip (about 80–95 %). On both tips, the oscillations of

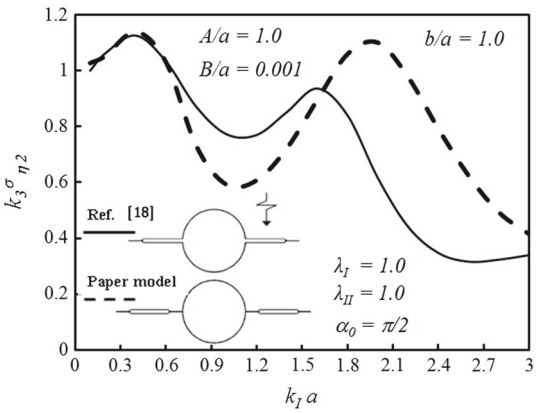

Fig. 3 DSIFs comparison between two models under vertical incidence

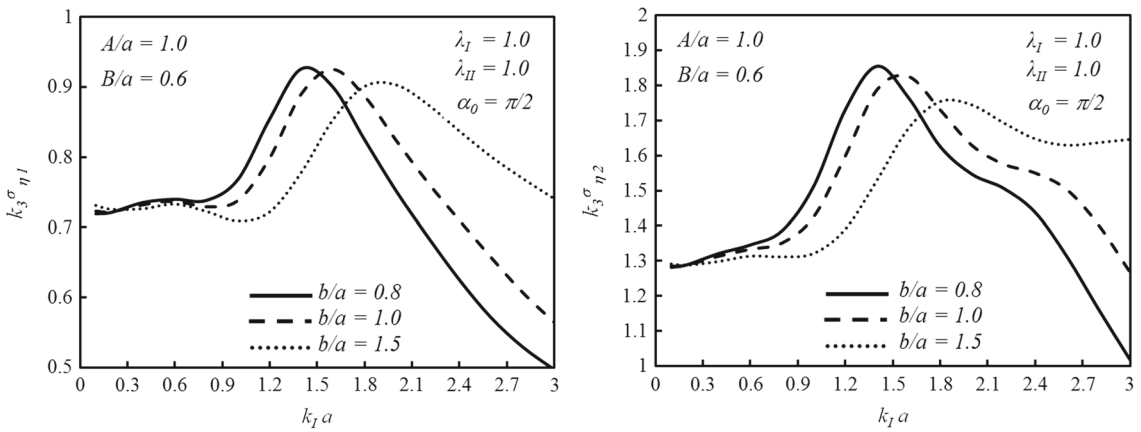

Fig. 4 DSIFs at η_1 and η_2 versus $k_I a$ for different semi-axes' percentages of the ellipse

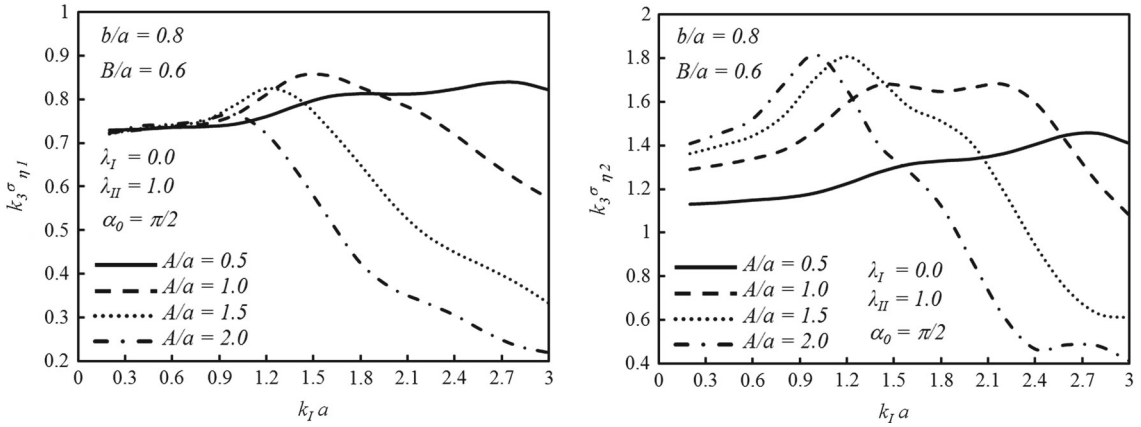

Fig. 5 DSIFs at η_1 and η_2 versus $k_{\mathrm{I}}a$ for different A/a percentages

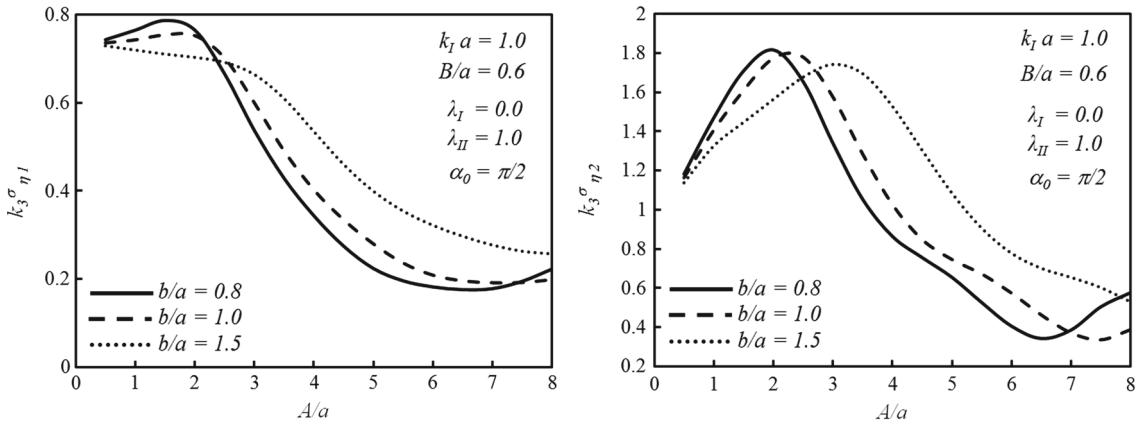

Fig. 6 DSIFs at η_1 and η_2 versus A/a percentage for different semi-axes' percentages of ellipse

the curves started to be clear at $k_{\mathrm{I}}a > 0.6$. The peak of the curves occurred at almost the same $k_{\mathrm{I}}a$ percentages for the two tips' curves. Then, the DSIFs continue to decrease rapidly with $k_{\mathrm{I}}a$ increment. But when $b/a = 1.5$, the decrement occurr slowly. So, the increment of the semi-axes' percentage leads to the decrement of both the curve's peak and the variation of DSIFs with $k_{\mathrm{I}}a$.

Variations of DSIFs at η_1 and η_2 for different A/a percentages are shown in Fig. 5. The semi-axes' percentage is $b/a = 0.8$.

On the inner tip, the variations of the curves started to be clear at $k_{\mathrm{I}}a > 0.9$. The curve for the percentage $A/a = 0.5$ showed a very little increase in DSIFs with the increment of $k_{\mathrm{I}}a$. While the percentage A/a increased, the curve showed higher oscillation and a rapid decrease of the DSIFs. On the outer tip, while the percentage A/a increased, the peak value of the curve increased and the DSIFs decreased rapidly.

Divergences of DSIFs at η_1 and η_2 for different semi-axes' percentages of the ellipse are shown in Fig. 6. The outer tip gave larger values of DSIFs than the inner tip. The peak of the curves occurred at almost the same A/a percentages for the two tips' curves. In the inner tip, the peak value decrease with the increment of the b/a percentage. In the outer tip, the peak value decrement is small. The DSIFs curves continue to decrease rapidly with the A/a increment. But, the values of DSIFs are larger for $b/a = 1.5$ for the two tips' curves. So, the DSIFs decreased with the increment of the A/a, for different semi-axes' percentages, and the semi-axes' percentage of the ellipse $b/a = 1.5$ gave the smaller peaks and the larger values of DSIFs for the two tips.

Variations of DSIFs at η_1 and η_2 for different incident wave frequencies (λ_{I}) are shown in Fig. 7. The curves at the inner tip almost coincide while λ_{I} changes. But at the outer tip, the difference between the curves is clearer. On both tips, the DSIFs curves continue to decrease rapidly while $A/a > 2$. So, the DSIFs decreased with the increment of A/a for different incident wave frequencies.

It can be concluded that the rise of the incident wave number harms the efficiency of piezoelectric devices and materials used, especially when the crack length is longer than twice the elliptic cavity's semi-axis a.

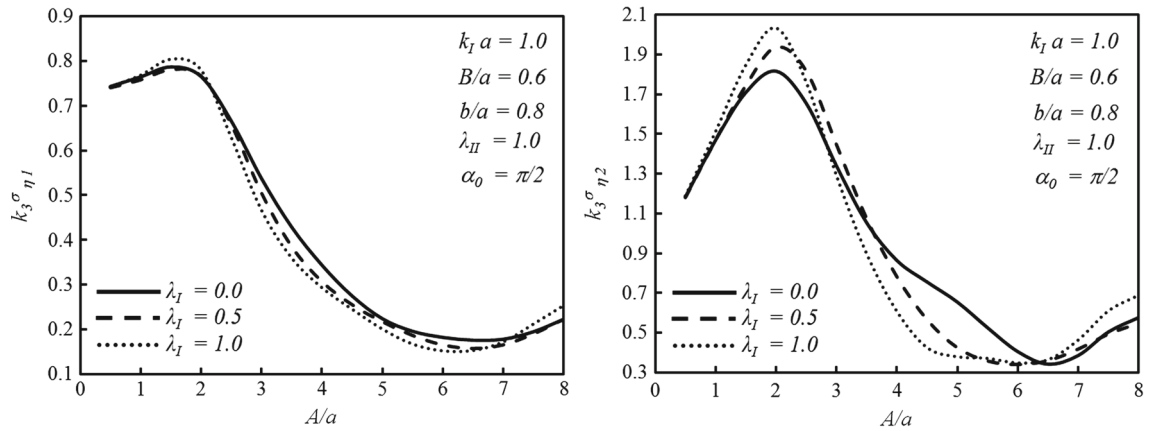

Fig. 7 DSIFs at η_1 and η_2 versus A/a percentage for different wave frequencies

7 Conclusions

A theoretical analysis is followed to calculate the DSIFs due to the existence of symmetrically radial cracks near the edges of a non-circular cavity, in transversely isotropic piezoelectric bi-materials. The model is considered under dynamic SH-wave. Based on complex variable and conformal mapping methods, Green's functions are constructed, and the DSIFs at the cracks' inner and outer tips are obtained by conjunction and cracks-deviation techniques. Numerical calculations are provided with an elliptic cavity based on FORTRAN language program. Calculating results clarified that, depending on the medium's geometry and the sequence of calculations, the relation between the cracks and the cavity is altered causing the changes occurring to the values of the DSIFs. The outer tip gave the larger values of DSIFs than the inner tip in all cases of study. The increment of the semi-axes' percentage led to the decrement of both the curve's peak and the DSIFs variation with the wave number. The DSIFs decreased with the increment of the crack length ratio for both the different semi-axes' percentages and the different incident wave frequencies. The rise of the incident wave number harms the efficiency of piezoelectric devices and materials used, especially when the crack length is longer than twice the elliptic cavity's semi-axis a.

References

1. Qin, Q.H.: Green's function and its application for a piezoelectric plate with various openings. Arch. Appl. Mech. **69**, 133–144 (1999)
2. Wu, L.Z.: A crack in a confocal elliptic piezoelectric in-homogeneity embedded in an infinite piezoelectric medium. Int. J. Fract. **104**, 1–14 (2000)
3. Liu, J.X., Wang, X.Q.: Interaction of a screw dislocation with a notch in a piezoelectric bi-material. Arch. Appl. Mech. **73**, 553–560 (2004)
4. Sasaki, T., Suzuki, T., Hirashima, K.: Transversely isotropic piezoelectric materials with an arbitrarily shaped boundary. Acta Mech. **184**, 217–230 (2006)
5. Gui, Z.J., Hu, H.P., Yang, F.: Interaction between collinear periodic cracks in an infinite piezoelectric body. Appl. Math. Mech. (English Edition) **29**, 863–870 (2008)
6. Guo, J.H., Lu, Z.X., Han, H.T., Yang, Z.: The behavior of two non-symmetrical permeable cracks emanating from an elliptical hole in a piezoelectric solid. Eur. J. Mech. A/Solids **29**, 654–663 (2010)
7. Guo, J.H., Lu, Z.X., Feng, X.: The fracture behavior of multiple cracks emanating from a circular hole in piezoelectric materials. Acta Mech. **215**, 119–134 (2010)
8. Chen, Z., Liu, D., Yang, Z.: Dynamic stress concentration and scattering of SH-wave by interface elliptic cylindrical cavity. Earthq. Eng. Eng. Vib. **2**, 299–306 (2003)
9. Liu, D., Chen, Z.: Scattering of SH-wave by cracks originating at an elliptic hole and dynamic stress intensity factor. Appl. Math. Mech. **25**, 1047–1056 (2004)
10. Liu, D., Lin, H.: Scattering of SH-waves by an interacting interface linear crack and a circular cavity near bio-material interface. Acta Mech. Sin. **20**, 317–326 (2004)
11. Wu, X.F., Dzenis, Y.A.: Screw dislocation interacting with an interfacial edge crack between two bonded dissimilar piezoelectric wedges. Int. J. Fract. **117**, L9–L14 (2002)
12. Chen, S., Shen, M., Chen, F.: Piezoelectric study on elliptic in-homogeneity problem using alternating technique. J. Elast. **81**, 91–109 (2005)

13. Rogowski, B.: The mode III cracks emanating from an elliptical hole in the piezo-electro-magneto-elastic materials. Arch. Appl. Mech. **81**, 1607–1620 (2011)
14. Lu, Z.X., Liu, P., Guo, J.H.: Exact solutions of two semi-infinite collinear cracks in piezoelectric strip. Appl. Math. Mech. **32**, 1399–1406 (2011)
15. Guo, J., Lu, Z.: Fracture behavior of two non-symmetrical collinear cracks emanating from an elliptical hole in a piezoelectric material. Frontiers Mech. Eng. **6**, 296–300 (2011)
16. Xiao, J.H., Xu, Y.L., Zhang, F.C.: Interaction between periodic cracks and periodic rigid-line inclusions in piezoelectric materials. Acta Mech. **224**, 777–787 (2013)
17. Song, T.S., Sun, L., Liu, D.: Dynamic anti-plane characteristic of an infinite piezoelectric medium with a non-circular cavity. ASME 2005 International Design Engineering Technical Conferences and Computers and Information in Engineering Conference, California, USA (2005)
18. Song, T.S., Dong, L.: Dynamic stress intensity factor for interfacial cracks of mode III on a circular cavity in piezoelectric bi-materials. Chin. J. Theor. Appl. Mech. **42**, 1219–1224 (2010)